# Investigating Enhanced Electrical Conductivity in Ice VII

Elvita Meskauskaite*[1], Miriam Peña Alvarez†[1], Israel Osmond[1]

[1] School of Physics and Astronomy, University of Edinburgh

**Open Access**

**Received**
19 Sep 2024

**Revised**
29 Sep 2024

**Accepted**
08 Oct 2024

**Published**
24 Oct 2024

**Abstract**

At ambient conditions, the electrical conductivity of $H_2O$ is around 0.01 S/m, whereas in the deep interiors of Neptune and Uranus ($\approx$ 5000 K and $\approx$ 300 GPa), conductivity increases by three orders of magnitude. So far, few experimental studies have considered the conductivity properties of ice at high-$P$-$T$ conditions. In this work, we evaluate how the conductivity of $H_2O$ changes upon compression at 300 K, and show that at 10 GPa, ice VII exhibits a maximum in conductivity of $1.43 \pm 0.47 \times 10^{-5}$ S/m. We propose that time is an important variable in impedance spectroscopy measurements during the pressure-induced transitions: fluid $\rightarrow$ phase VI $\rightarrow$ phase VII, between 0.5 and 4 GPa.

**DOI**: 10.2218/esjs.9994 **ISSN** 3049-7930

## Introduction

Voyager 2 revealed that the magnetic fields of Uranus and Neptune are non-dipolar and non-axisymmetric, a phenomenon still poorly understood today (Stone *et al.* 1989). It is hypothesised that the interiors of these planets, composed of $CH_4$, $NH_3$, and $H_2O$, host $H_2O$ in a superionic phase under extreme conditions ($\approx$ 5000 K and $\approx$ 300 GPa) (Hubbard 1997; Teanby *et al.* 2020). In this phase, hydrogen ions diffuse rapidly through a *bcc* (body-centred cubic) lattice, resulting in electrical conductivities exceeding 10 S/m (Cavazzoni *et al.* 1999). Shock compression experiments suggest that superionic ice possesses sufficient conductivity to generate the magnetic fields observed by Voyager 2 (David *et al.* 1959). Convective motions driven by internal heat may induce electric currents, contributing to the planetary dynamo. Understanding this dynamo process requires further study of the electrical conductivity of ices (Helled *et al.* 2020).

Sugimura *et al.* (2012) were the first to experimentally study superionic ice using a diamond anvil cell (DAC) at $T = 739$ K, $P = 56$ GPa, and $T = 749$ K, $P = 62$ GPa, reporting a conductivity of 10 S/m. Other methods, such as shock compression (Millot *et al.* 2018) and X-ray diffraction (Prakapenka *et al.* 2021) have also explored superionic ice, however, due to the experimental challenges at extreme pressure-temperature ($P$-$T$) conditions, its properties remain underexplored. Lin *et al.* (2005) investigated the melting behaviour of $H_2O$ under high-$P$-$T$, identifying a triple point between fluid $H_2O$, ice VII, and superionic ice using Raman spectroscopy and X-ray diffraction. This work focuses on developing a technique to examine the electrical properties of $H_2O$ as it compresses to ice VII at room temperature.

Upon compression at 300 K, a series of phase transitions in $H_2O$ has been confirmed: fluid $H_2O$ transitions to ice VI at 1 GPa, and further compression to 2.2 GPa forms ice VII (Noguchi *et al.* 2016). Hydrogen-bond symmetrisation leads to a transition from ice VII to a disordered phase (VII') at 40 GPa, with phase X forming at 66 GPa (Wolanin *et al.* 1997), as observed by X-ray diffraction, neutron studies, and density-functional calculations (Sugimura *et al.* 2008; Komatsu *et al.* 2024).

Phase VI has a tetragonal structure with disordered hydrogen atoms, allowing proton movement (Kamb 1965). Ice VII has a *bcc* structure with a denser hydrogen-bonded network (Kamb *et al.* 1964). Proton transport in the *bcc* oxygen lattice of ice is responsible for its electrical conductivity (Decroly *et al.* 1957; Jaccard 1959) and it involves transitions along hydrogen bonds, creating ionic defects ($H_3O^+$ and $OH^-$)

*Student Author
†Corresponding academic contact: Miriam.Pena.Alvarez@ed.ac.uk

and Bjerrum defects (L or D) from bond to bond displacements (Jaccard 1964). Theoretical studies suggest ice VII's conductivity maximum is due to the transition from rotational to ionic defect carriers (Iitaka 2013).

The maximum conductivity of ice at 10 GPa and 300 K reported by Okada *et al.* (2014) has not been reproduced, however, between 20 and 40 GPa at 300 K, conductivity is found to be inconsistent with the work of Sugimura *et al.* (2012), which suggests that electrode geometry or impedance spectroscopy methods may affect the obtained conductivity. Using the methods of Okada *et al.* (2014), we investigate conductivity behaviour at pressure-induced transitions: fluid → phase VI → phase VII, and their time dependence. Comparison with literature values allows us to identify the limiting factors in these methods. Additionally, we present electrical conductivity measurements of $H_2O$ under pressures from 0.4 to 15 GPa at 300 K, using a diamond anvil cell (DAC) along with Raman and impedance spectroscopy. A conductivity maximum for ice VII is observed at $P_c = 10$ GPa and 300 K.

## Methods

The DAC was prepared with a 200 $\mu m$ diamond culet. A rhenium (Re) gasket was pre-indented and laser-drilled to create a sample chamber for Milli-Q water, insulated with $Al_2O_3$ and low-viscosity epoxy for electrical measurements. Tungsten (W) and gold (Au) electrodes were sputtered using the Korvus HEX magnetron sputtering system, with thicknesses of 1600 Å and 800 Å, respectively.

Ahmed *et al.* (2010) showed that the electrode's active area affects AC impedance in the low-frequency region. Initially, no peak in conductivity was observed with smaller active-area electrodes, as shown in the left panel of Figure 1(a). Redesigning the electrodes to increase proton transport pathways within ice grain boundaries, as shown in the right panel, led to improved results. Electrical contact between the electrodes and the cell was avoided. Impedance measurements were taken using a Hioki "LCR Meter 3536" with a frequency range of 4-8 MHz at 1 V for each pressure step.

Pressure monitoring was done via Raman spectroscopy using a 514.35 nm Argon laser and a PyLoN:100 CCD camera from Princeton Instruments. A 300 lines/mm grating was used to measure the OH stretching mode, and for pressures above 5 GPa, the Raman shift of the stressed diamonds' high-frequency edge was measured using an 1800 lines/mm grating (Hanfland *et al.* 1985).

## Results & Discussion

Figures 1(b) and (c) show the pressure dependence of the OH stretching mode during compression. Phase transitions were identified based on (Hsieh *et al.* 2015), using the dominance and Raman shift of symmetric and asymmetric OH stretching modes. As fluid $H_2O$ transitions to phase VI, the asymmetric OH stretching mode is less prominent, allowing the Raman shift of the in-phase symmetric stretch mode to be used for monitoring pressure beyond this transition.

Figure 1(d) shows a Nyquist plot obtained during a 10-minute compression run with a defined semicircle arc and a Warburg impedance tail. The arc diameter is found to increase with pressure, meaning that the bulk resistance increases. It is unexpected that above 2.3 GPa, one still identifies a Warburg tail, as the disappearance of the tail would suggest that the sample transitions from a more diffusive phase to a less diffusive phase, i.e., fluid $H_2O$ → phase VI, VII. We infer that the observation of the Warburg tail is a result of the sample not achieving a steady state. This means that the impedance measurement does not reflect the equilibrium properties of the sample and is affected by factors such as an ongoing phase transition, rearrangement of the hydrogen bond network, or non-linear responses arising from the polarisation of the sample close to electrodes. However, during a decompression run, a sufficient amount of time was given for the sample to equilibrate, hence the disappearance of the tail past 1 GPa, which is in agreement with the fluid $H_2O$ → phase IV transition. Figure 1(e) shows impedance spectra for a decompression run where the bulk resistance arc is less defined due to a greater effect of the electrical double layer (EDL) capacitance.

In phases VI and VII, complex impedance spectra were limited in the low-frequency region due to the EDL capacitance (Ariyoshi *et al.* 2022) as shown in Figure 1(f). Hence, an equivalence circuit fitting technique was used. This method relies on selecting circuit components to form a circuit which reflects the electrical properties of the tested system (Wang *et al.* 2021). The equivalence circuit with the resistor

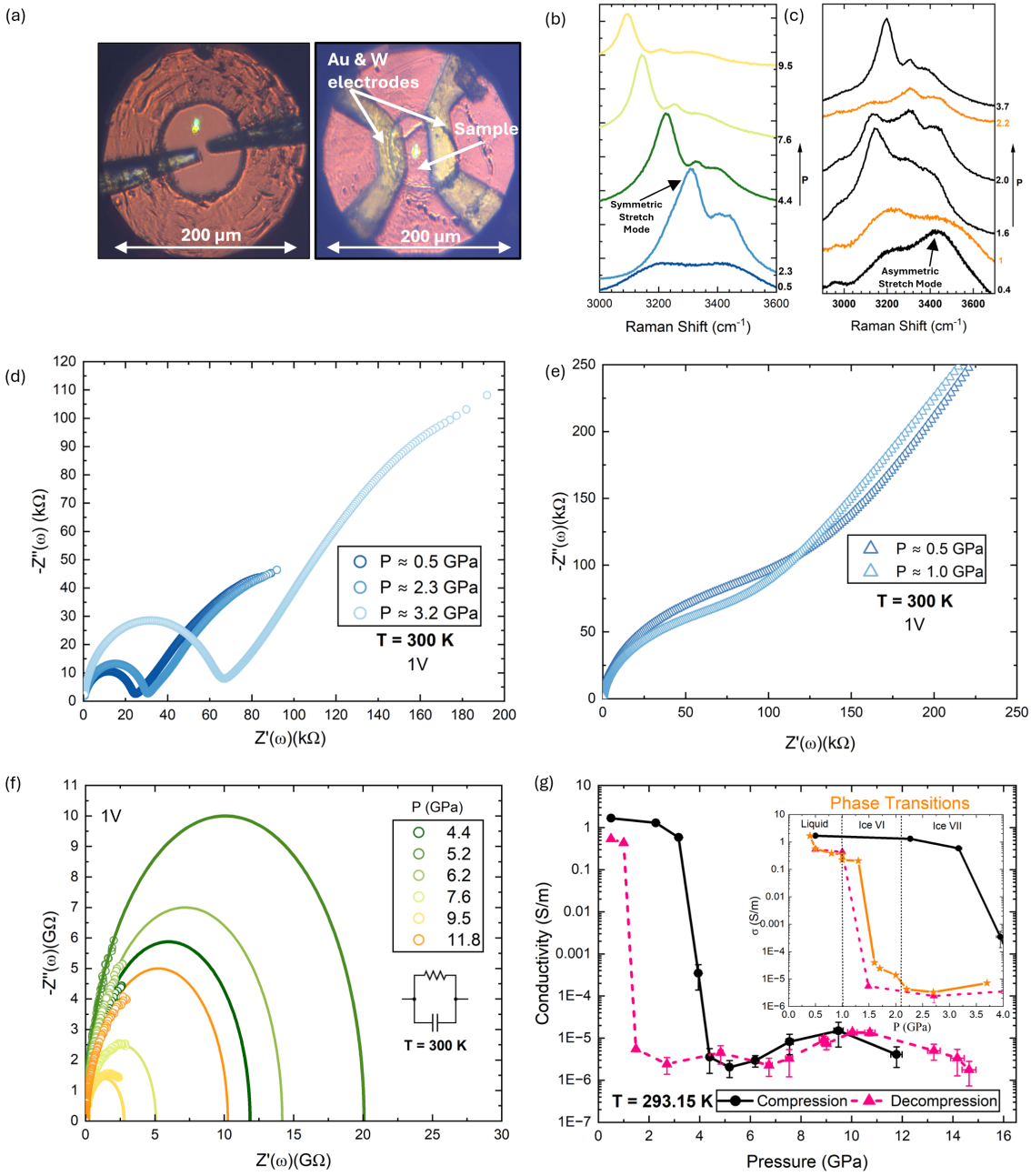


Figure 1: **(a)** Microscopic images of the sample and electrodes in the DAC. Left: Electrode geometry which did not produce a maximum in conductivity. Right: Improved electrode geometry with a greater active area. The sample chamber shows a phase transition from fluid $H_2O$ → ice VI. **(b)** The OH stretching modes are colour-coded to match the complex impedance spectra shown in (d) and (f) for a compression run. **(c)** Raman spectra in the region of OH stretching bands as a function of pressure during the "Phase Transitions" run shown in the inset of (g). **(d)** Nyquist plot of complex impedance spectra for 0.5 GPa < P < 3.2 GPa, which covers the transitions: fluid $H_2O$ → ice VI → ice VII. **(e)** Nyquist plot of complex impedance spectra for a decompression run. **(f)** An equivalence circuit fitting of complex impedance spectra for pressure range, 4.4 GPa < P < 11.8 GPa. The equivalence circuit was chosen to be a resistor in parallel to a capacitor. Resistance values for each pressure step obtained with these fits were used to calculate conductivity values plotted in the following panel. **(g)** Conductivity is calculated from the resistance and dimensions measured for each run and each pressure for both compression and decompression cycles. Inset: Conductivity values in orange represent a repeated compression run, for obtaining more data points covering the phase transition region.

(R) and capacitor (C) in parallel was chosen; see inset of Figure 1(f). The impedance equation of the equivalence circuit used for the fitting is:

$$Z = \frac{R}{1 + (i\omega)^p RC} \tag{1}$$

where the fitting parameter, $p = 1$, represents an ideal capacitor behaviour and is chosen for simplifying the data analysis. Angular frequency, $\omega$, is expressed as $\omega = 2\pi f$, where $f$ is frequency.

The conductivity of ice, $\sigma$, was determined by equation $\sigma = d/(R \times l \times t)$, where $d$ is the distance between electrodes, $l$ is the diameter of the sample chamber, and $t$ is the *in situ* thickness of the sample. $R$ is the bulk sample resistance which is determined from the diameter of the arc taken from the fitting shown in Figure 1(f).

In Figure 1(g), we have presented the calculated conductivity for all of our pressure points as a function of pressure. A maximum in conductivity of $1.43 \pm 0.47 \times 10^{-5}$ S/m is observed during compression and decompression runs at $P_c \approx 10$ GPa and 300 K. Okada *et al.* (2014) obtained a maximum in conductivity between $10^{-5}$ and $10^{-6}$ S/m at 10 GPa, which is in agreement with our result. Between 2 and 4 GPa, in which the transition VI $\rightarrow$ VII is present, they obtained $10^{-7} < \sigma < 10^{-5}$ S/m. However, in the same pressure region, as shown in the inset of Figure 1(g), we obtained higher conductivity by two orders of magnitude. Okada *et al.* (2014) did not investigate fluid $H_2O \rightarrow$ phase VI transition, therefore, our results cannot be compared. However, in this transition region below 1 GPa, fluid $H_2O$ exhibits conductivity of 0.01–1 S/m, which agrees with literature values of Jones (2002). Positive conductivity dependence of pressure observed by Zheng *et al.* (1997) is inconsistent with our result; on the contrary, the conductivity was found to decrease.

Sugimura *et al.* (2012) obtained $10^{-5} < \sigma < 10^{-4}$ S/m from 20 to 40 GPa at 300 K, and $\sigma \approx 10^{-5}$ S/m at 40 GPa, whereas Okada *et al.* (2014) obtained $10^{-6} < \sigma < 10^{-5}$, and $10^{-7} < \sigma < 10^{-6}$, respectively. These results differ by around two orders of magnitude which is significant when interpreted in the context of superionic conduction.

Given our discrepancies at the phase transitions, and those between previous works by Sugimura *et al.* (2012) and Okada *et al.* (2014), we propose that the inconsistency in the results is due to the electrode geometry and the sample not reaching a steady state. Our preliminary results using electrode configuration shown in the left panel of Figure 1(a) would cause a drift in conductivity and omission of the maximum of conductivity upon compression. However, once the configuration was changed as shown in the right panel of Figure 1(a) the maximum was achieved, indicating that electrode geometry has a significant effect on impedance spectroscopy technique. Secondly, the aforementioned steady-state must also be achieved in order to obtain reliable impedance measurements. However, the effect on conductivity on a single ice phase structure is dependent on pressure. Thus, if a mixture of phases is present, small inevitable pressure gradients may fluctuate the overall conductivity of the sample as well.

## Conclusion

We have experimentally found a maximum in electrical conductivity of ice VII at 10 GPa and 300 K, for both compression and decompression runs, using a DAC, through Raman and Impedance spectroscopy techniques. We suggest that electrode geometry and the effect of time-dependent phase transitions on impedance spectroscopy are responsible for the inconsistencies in obtained conductivity in the phase transition dominant pressure region and literature results.

## Acknowledgements

I would like to thank Dr Miriam Peña Alvarez and Dr Israel Osmond for their help and support throughout the project, as well as the journal editors and reviewers for their feedback. This project was made possible and funded by the Carnegie Scholarship and the UKRI Future Leaders Fellowship No. Mrc-Mr/T043733/1.

## References


Ahmed, R. and Reifsnider, K. 'Study of Influence of Electrode Geometry on Impedance Spectroscopy' in 2010 8th International Conference on Fuel Cell Science, Engineering and Technology (The American Society of Mechanical Engineers; 2010)

Ariyoshi, K. *et al.* 'Electrochemical Impedance Spectroscopy Part 1: Fundamentals' Electrochemistry **90** 10 (2022)

Cavazzoni, C *et al.* 'Superionic and Metallic States of Water and Ammonia at Giant Planet Conditions' Science **283** 5398 (1999)

David, H. G. and Hamann, S. D. 'The Chemical Effects of Pressure. Part 5. The Electrical Conductivity of Water at High Shock Pressures' Transactions of the Faraday Society **55** (1959)

Decroly, J. *et al.* 'Caractére de la Conductivité électrique de la Glace' Helvetica Physica Acta **30** (1957)

Hanfland, M and Syassen, K 'A Raman Study of Diamond Anvils Under Stress' Journal of Applied Physics **57** 8 (1985)

Helled, R. *et al.* 'Uranus and Neptune: Origin, Evolution and Internal Structure' Space Science Reviews **216** 3 (2020)

Hsieh, W. and Chien, Y. 'High Pressure Raman Spectroscopy of H2O-CH3OH Mixtures' Scientific Reports **5** 1 (2015)

Hubbard, W. 'Neptune's Deep Chemistry' Science **275** 5304 (1997)

Iitaka, T 'Simulating Proton Dynamics in High-Pressure Ice' The Review of High Pressure Science and Technology **23** 2 (2013)

Jaccard, C. 'Étude Théorique Et Expérimentale Des Propriétés électriques de la Glace' (1959)

Jaccard, C. 'Thermodynamics of Irreversible Processes Applied to Ice' Physik der kondensierten Materie **3** 2 (1964)

Jones, R. 'Measurements of the Electrical Conductivity of Water' IEE Proceedings-Science, Measurement and Technology **149** 6 (2002)

Kamb, B. 'Structure of Ice VI' Science **150** 3693 (1965)

Kamb, B. and Davis, B. L. 'Ice VII, the Densest Form of Ice' Proceedings of the National Academy of Sciences **52** 6 (1964)

Komatsu, K. *et al.* 'Hydrogen Bond Symmetrisation in D2O Ice Observed by Neutron Diffraction' Nature Communications **15** 1 (2024)

Lin, J.-F. *et al.* 'Melting Behavior of H2O at High Pressures and Temperatures' Geophysics Research Letters **32** 11 (2005)

Millot, M. *et al.* 'Experimental Evidence for Superionic Water Ice Using Shock Compression' Nature Physics **14** 3 (2018)

Noguchi, N. and Okuchi, T. 'Self-Diffusion of Protons in H2O Ice VII at High Pressures: Anomaly Around 10 GPA' The Journal of Chemical Physics **144** 23 (2016)

Okada, T. *et al.* 'Electrical Conductivity of Ice VII' Scientific Reports **4** 1 (2014)

Prakapenka, V. B. *et al.* 'Structure and Properties of Two Superionic Ice Phases' Nature Physics **17** 11 (2021)

Stone, E. C. and Miner, E. D. 'The Voyager 2 Encounter With the Neptunian System' Science **246** 4936 (1989)

Sugimura, E. *et al.* 'Compression of H 2 O Ice to 126 GPA and Implications for Hydrogen-Bond Symmetrization: Synchrotron X-ray Diffraction Measurements and Density-Functional Calculations' Physical Review B **77** 21 (2008)

Sugimura, E. *et al.* 'Experimental Evidence of Superionic Conduction in H2O Ice' The Journal of Chemical Physics **137** 19 (2012)

Teanby, N. A. *et al.* 'Neptune and Uranus: Ice or Rock Giants?' Philosophical Transactions of the Royal Society A **378** 2187 (2020)

Wang, S. *et al.* 'Electrochemical Impedance Spectroscopy' Nature Reviews Methods Primers **1** 1 (2021)

Wolanin, E. *et al.* 'Equation of State of Ice VII Up to 106 GPA' Physical Review B **56** 10 (1997)

Zheng, H. *et al.* 'The Electrical Conductivity of H2O at 0.21-4.18 GPA and 20-350 C' Chinese Science Bulletin **42** 12 (1997)